WELDING RESEARCH

SUPPLEMENT TO THE *WELDING JOURNAL*, SEPTEMBER 2023
Sponsored by the American Welding Society

Application of Digital Image Correlation in Cross Weld Tensile Testing: Test Method Validation

The objectives of this study included validation of DIC-instrumented tensile testing methodology for use in CWTT and more

BY W. SIEFERT, B. ALEXANDROV, AND M. BUEHNER

Abstract

This study addresses the limitations of cross weld tensile testing (CWTT) in quantifying local mechanical properties across microstructural and compositional gradients in dissimilar– and matching–filler metal welds. A digital image correlation (DIC) methodology was validated for application in CWTT by direct comparison of stress-strain curves generated using conventional and virtual DIC extensometers in tensile testing of homogeneous steel samples.

DIC-instrumented CWTT of dissimilar weld metal Alloy 625 filler metal on F65 steel demonstrated capability in quantifying the local yield strength, strain-hardening kinetics, and strain at failure in the base metal, heat-affected zone (HAZ), fusion boundary (FB) region, and weld metal in dissimilar and matching filler metal welds. It was shown that the high strain-hardening capacity in Alloy 625 weld metal led to base metal failure in CWTT despite the lower Alloy 625 weld metal yield strength. It was also shown that DIC-instrumented CWTT can be used for determining weld metal undermatching and overmatching conditions in compositionally matching- and dissimilar-metal welds. Furthermore, by quantifying local strain distribution (both elastic and plastic) in the HAZ, FB region, and weld metal, DIC-instrumented CWTT provides an additional method for evaluating hydrogen-assisted cracking susceptibility in dissimilar-metal welds.

Keywords

- Digital Image Correlation (DIC)
- Dissimilar-Metal Welds (DMWs)

https://doi.org/10.29391/2023.102.015

Introduction

Tensile testing offers a destructive method for determining strength and ductility in metallic alloys (Refs. 1–4). These properties are fundamental in the process of materials selection and in qualification of manufactured components for service (Refs. 5, 6). The engineering stress and strain data generated in tensile testing are defined on the assumption of uniform stress and strain distribution in a gauge section of standardized geometry (Refs. 1–4). Strain measurements over standardized gauge lengths are used for determining the yield strength (YS) and the overall ductility of the tested material (Refs. 1–4). Mechanical extensometers used for strain measurement must be physically attached to the sample, have limited extension ranges, and may slip or damage during testing.

Cross weld tensile testing (CWTT) is used in welding procedure qualification for determining the ultimate tensile strength (UTS) of weldments and validating weld metal (WM) quality through confirming base metal (BM) failure (Refs. 1–6). YS is not determined in CWTT due to expected gradients in mechanical properties and nonuniform straining response in the BM, heat-affected zone (HAZ), and WM (Ref. 1) as well as the inability of conventional extensometers to measure local strain (Refs. 7–19, 21–23).

Digital image correlation (DIC) offers a contactless method for strain measurement in materials testing (Refs. 7–19, 22, 23). DIC utilizes a randomized speckle pattern applied to a test sample surface. The speckles' relative displacement during straining is continuously imaged and recorded during testing. Specialized software analyzes the recorded speckles' relative displacement using image matching algorithms to quantify the temporal and spatial strain distribution (Refs. 13–16). High accuracy of strain measurement can be achieved with proper DIC procedures (Ref. 16).

Numerous examples of DIC application in materials testing exist (Refs. 7–13, 18, 19, 22, 23). However, the use of this method in CWTT is surprisingly limited (Refs. 7–9, 12, 13).

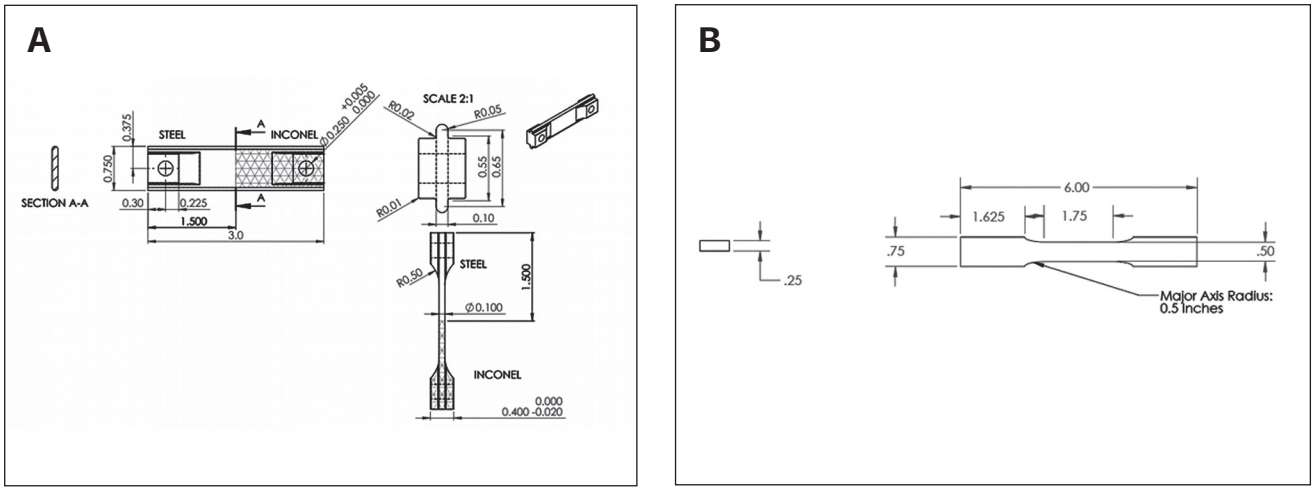

Fig. 1 — Tensile test sample geometries: A — F65/625 CWTT DHCT; B — F22 BM ASTM E8 dog bone.

Strain localization in materials has been demonstrated in most DIC studies (Refs. 7–13). Strain localization has led to observations of microstructures during straining and failure under tension (Refs. 7, 10, 11) and the role of the local microstructure in localized strain gradients. Of particular interest are the kinetics of strain accumulation and localization in dissimilar-metal welds (DMWs) (Refs. 7, 8) and along the fusion boundary (FB) of steel welds during interrupted tests (Ref. 11). DIC has enabled studying other straining mechanisms in welds, such as strain ratcheting (Ref. 13).

DIC strain measurement is highly local (Refs. 7–19), which is expected to allow quantification of the local mechanical behavior across compositional, microstructural, and property gradients (Ref. 20) during CWTT of dissimilar– and matching–filler metal welds (Ref. 7). The objectives of this study included: 1) validation of DIC-instrumented tensile testing methodology for use in CWTT; 2) determining the applicability of BM YS, measured per ASTM E8, *Standard Test Measures for Tension Testing of Metallic Metals*, for load selection in the delayed hydrogen cracking test (DHCT); and 3) demonstration of DIC capability in determining the local YS, kinetics of strain hardening, and strain at failure in the BM, HAZ, FB region, and WM in DMWs.

The DHCT has been developed for the evaluation of hydrogen-assisted cracking (HAC) susceptibility in DMWs (Ref. 24). It utilizes specific test sample geometry, with the dissimilar FB located in the middle of the gauge section, normal to the loading direction (Ref. 24). To accurately simulate HAC in service conditions, the test sample is subjected to a constant tensile load below the BM YS (Refs. 24–28).

Experimental Methodology

A BM of F22 steel (ASTM A182) and a DMW of F65 steel (ASTM A694) with Alloy 625 filler metal (ERNiCrMo-3) in the as-welded condition were subjected to tensile testing following the ASTM E8 testing procedure, simultaneously using a physical extensometer and multiple virtual DIC extensometers. The DMW joined two F65 forgings with 11-in. O.D. and 2.1-in. wall thickness using a 35-deg groove angle with a 0.04–0.08-in. root opening and was produced with the hot wire gas tungsten arc welding (GTAW-HW) procedure. The chemical compositions and the mechanical properties of the tested materials are shown in Tables 1 and 2, respectively.

Table 1 — Reported MTR Chemical Composition of Tested Materials in wt-%

Material	C	Mn	Si	P	S	Cr	Mo	Ni
F22 steel	0.14	0.52	0.19	0.005	0.002	2.36	1.01	0.16
F65 steel	0.17	1.21	0.23	0.013	0.005	0.10	0.024	0.10
ER NiCrMo-3	0.001	0.04	0.03	0.003	0.001	21.94	8.76	64.78

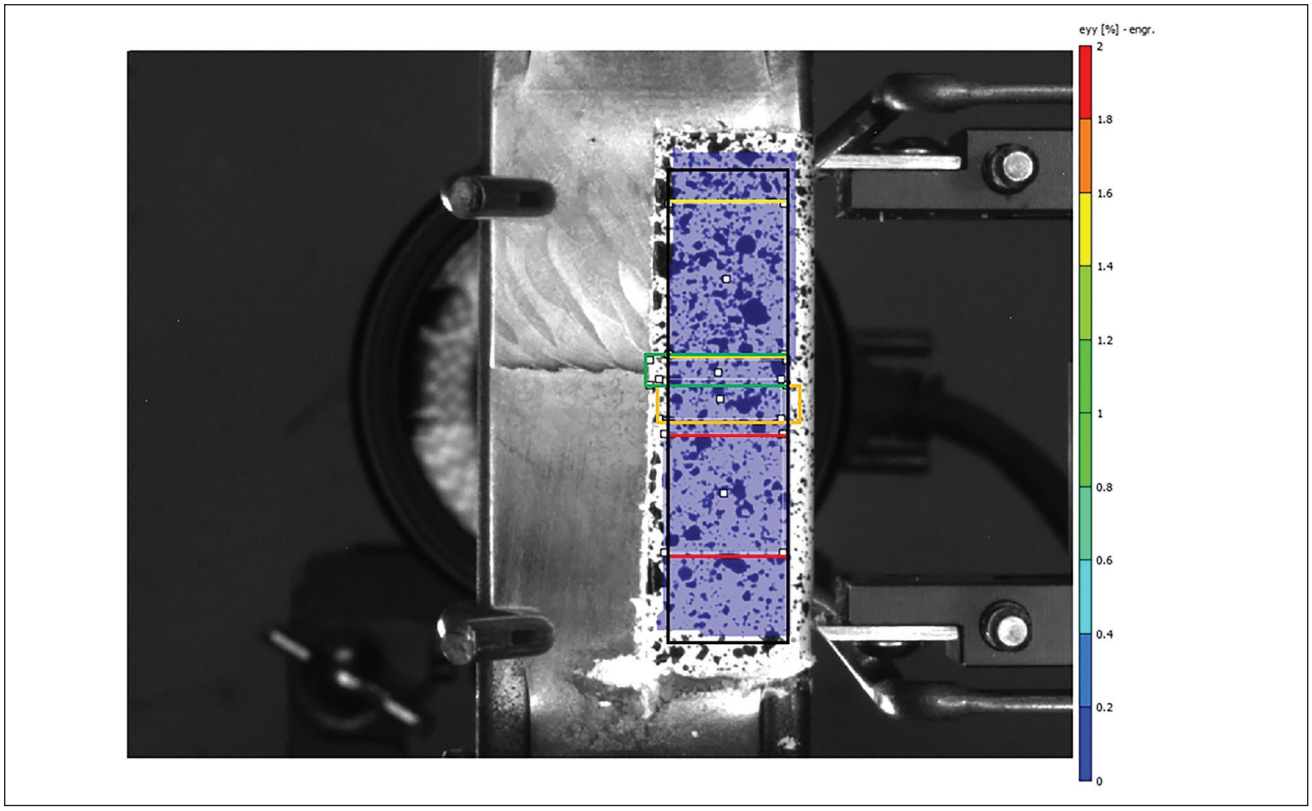

Fig. 2 — Etched F22/625 CWTT sample with applied DIC pattern. Also shown are the physical extensometer; the global DIC extensometer (black rectangle); and the BM, HAZ, FB, and WM local extensometers (red, orange, green, and yellow rectangles, respectively).

Two sample configurations were utilized: ASTM E8 dog bone geometry for the F22 BM tensile testing and NACE TM21453 DHCT geometry (Refs. 24–28) for both the F22 BM and the F65/625 DMW CWTT — Table 3 and Fig. 1. The DMW DHCT sample geometry utilized a FB centered at the sample gauge section and oriented perpendicular to the tensile loading direction. The samples tested in this study were extracted from a thick wall groove weld, where half of the sample was composed of steel BM and the other half was in the ERNiCrMo-3 WM.

The DHCT sample geometry was introduced in this study for two reasons: to discover how yield properties determined on an ASTM dog bone sample relate to the loading conditions in the DHCT and to explore the capacity of DIC in determining local mechanical properties in CWTT of DMWs. The DHCT applied a constant tensile load at stress levels that would avoid local yielding in the tested DMW at the onset of testing. The results of this study would demonstrate if BM YS determined by ASTM E8 can be used in determining the DHCT load.

Table 1 — continued

Material	Cu	V	Al	As	B	Nb
F22 steel	0.14	0.01	0.032	0.008	0.0002	0.005
F65 steel	0.29	0.085	0.015	0.005	0.0003	0.003
ER NiCrMo-3	0.02		0.15			3.57

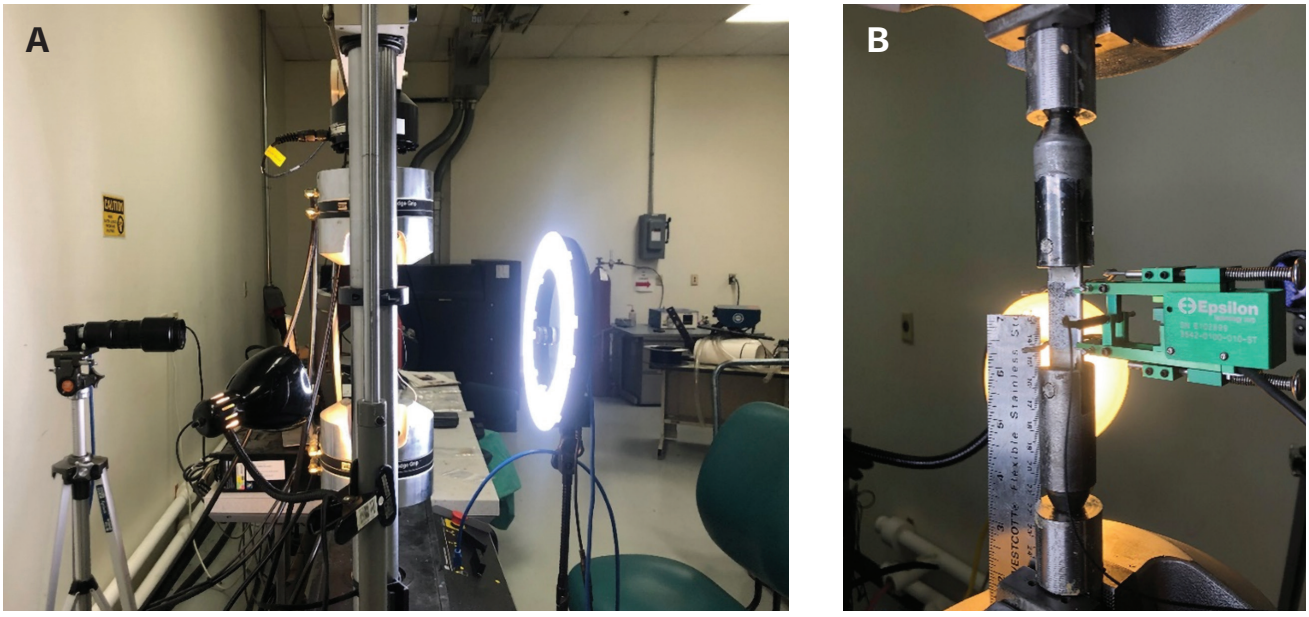

Fig. 3 — Tensile test setup: A — DIC with two cameras and lighting; B — DHCT sample attached to clevis and physical extensometer.

Table 2 — Mechanical Properties of Tested Materials (ASTM Minimum Specifications)

Materials	YS (ksi)	UTS (ksi)	Elongation (%)
F22 (ASTM A182)	≥ 75.0	≥ 95.0	≥ 17.0
F65 (ASTM A694)	≥ 65.0	≥ 77.0	≥ 20.0
IN625 (ERNiCrMo-3)	≥ 66.7	≥ 107.0	≥ 35.0

The test samples were extracted using electro-discharge machining. The gauge sections of the F65/625 CWTT samples were subjected to manual grinding (240 through 800-grit SiC paper) and polishing (9 through 1-micron diamond paste). These were etched using Kalling's reagent to reveal the BM, HAZ, FB, and WM regions and to allow for accurate placement of local extensometers in these regions. Half of the gauge sections of all test samples were painted with a DIC pattern, as shown in Fig. 2, while the other half was protected from painting by taping.

The tensile test setup included an MTS 810 test frame and an Epsilon 3542 1-in. +/– 10% extension extensometer — Fig. 3. Tensile testing was performed at a 0.001 in./s displacement rate through sample failure. Two FLIR Chameleon®3 cameras and two lamps were used for videotaping the DIC patterns during tensile testing. One of the cameras utilized a macro lens (10 frames/s capture rate) to record straining behavior over the whole gauge section of the tested samples. The other camera used a zoom lens (5 frames/s capture rate) for localized strain records in particular regions of interest. The DIC records were processed with VIC 2D commercial software to establish multiple virtual extensometers: 1) global in the gauge sections of the tested samples; 2) local in the expected necking area of the F22 BM samples; and 3) local in the BM, HAZ, FB region, and WM of the F65/625 CWTT samples.

The physical extensometer averaged the strain distribution over the entire 0.75-in.-wide, 1-in.-long gauge section. The virtual extensometers were defined over rectangular areas of interest as specified by their dimensions (width × length) in Table 3 and shown visually in Fig. 2. By averaging the strain over an area, such DIC extensometer setup reduces the noise in the DIC data and provides more accurate strain measurements (Refs. 7, 17). This is especially helpful when

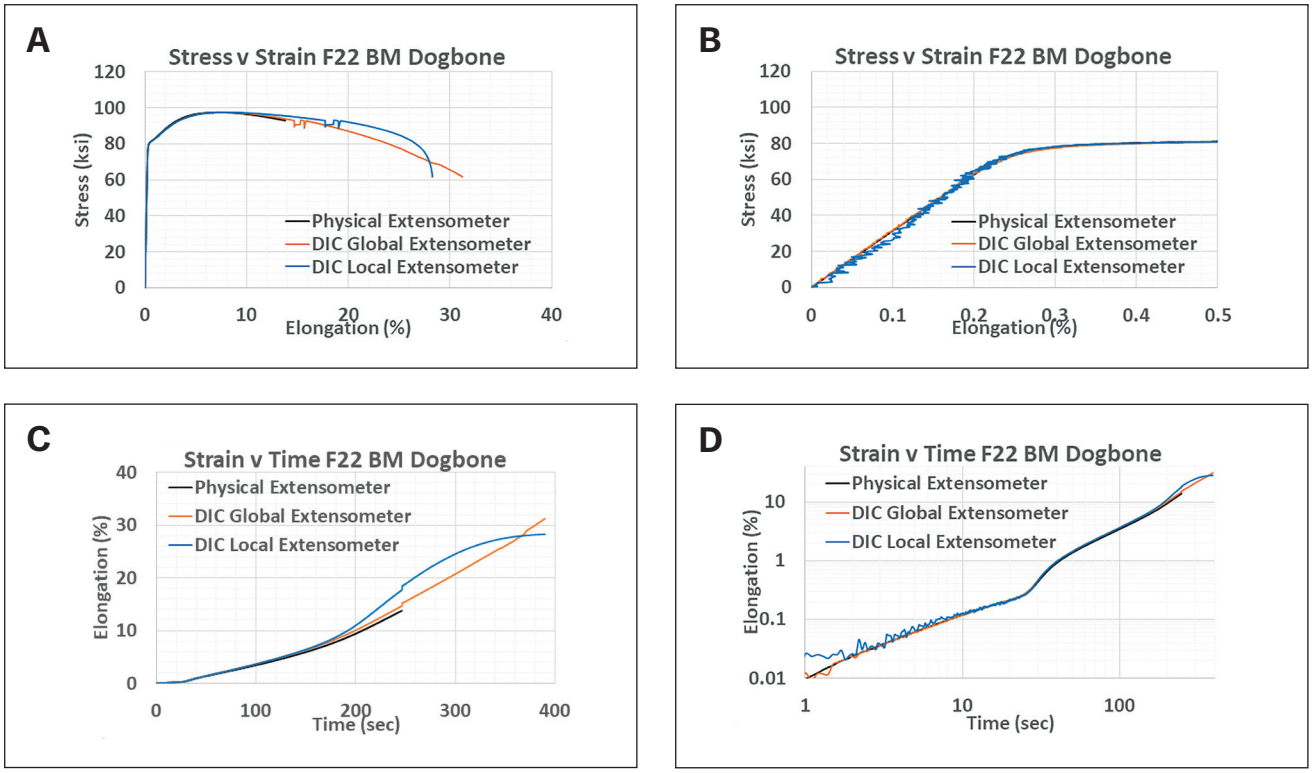

Fig. 4 — Comparison of DIC and physical extensometers in tensile testing F22 BM dog bone sample. A and B — Stress-strain curves; C and D — strain-time curves.

applied cross weld to determine the regional properties of welds (Table 5).

From the DIC tensile test results, simple calculations and results were obtained. First, YS was determined using a 0.2% offset line intercept method (Ref. 2). However, the YS determined was nonstandard due to the choice of testing rate (0.001 in./s displacement rate). This rate was chosen to allow a compromise between the standards and the desire to shorten testing times, which limits photo capture (and ultimate file sizes).

Elastic modulus was determined experimentally using the graphical data method (Ref. 3). However, for measurements within, it should be noted this is a nonstandard extensometer measurement. While the value itself is nonstandard, the comparison between extensometer calculations using standard measurement methods is useful to show agreement. The local DIC stress-strain curves were integrated to determine the mechanical energy absorbed during CWTT in the BM, HAZ, FB region, and WM.

Results

The results of this study are summarized in Tables 4 and 5. Specific examples of stress vs. strain and strain vs. time curves are shown in Figs. 4–6. Figures 4 and 5 and Table 4 compare the test results generated by physical, global DIC, and local DIC extensometers in the F22 BM dog bone and DHCT geometry samples. Note that the local DIC extensometers were located within the expected gauge section necking area. The goals of this comparison were: 1) validation of the global DIC extensometer with the physical extensometer; 2) quantification of the local straining behavior in the necking area, which could not be quantified by the global extensometers; and 3) determining the effect of sample geometry, ASTM dog bone vs. DHCT, on the determined YS.

Table 5 and Fig. 6 provide a quantitative comparison of the local mechanical behavior in terms of YS, strain, and strain hardening kinetics in the BM, HAZ, FB, and WM areas of the F65/625 DMW during CWTT. The objective was to demonstrate the capacity of DIC-instrumented CWTT in quantifying local mechanical behavior across compositional and microstructural gradients in a DMW.

Discussion

Physical Extensometer vs. DIC-Instrumented Tensile Test

The results in Table 4 show excellent agreement of the YS and modulus of elasticity, determined with the physical and DIC global extensometers, within each of the three tested F22 BM dog bone samples and among the DHCT samples. Note that the physical extensometer in dog bone sample 3 slipped, not allowing the determination of YS and modulus values. However, the DIC extensometer determined values of good agreement with dog bone samples 1 and 2.

The two samples with DHCT geometry, F22 BM and F65/625 CWTT, also showed very good agreement between

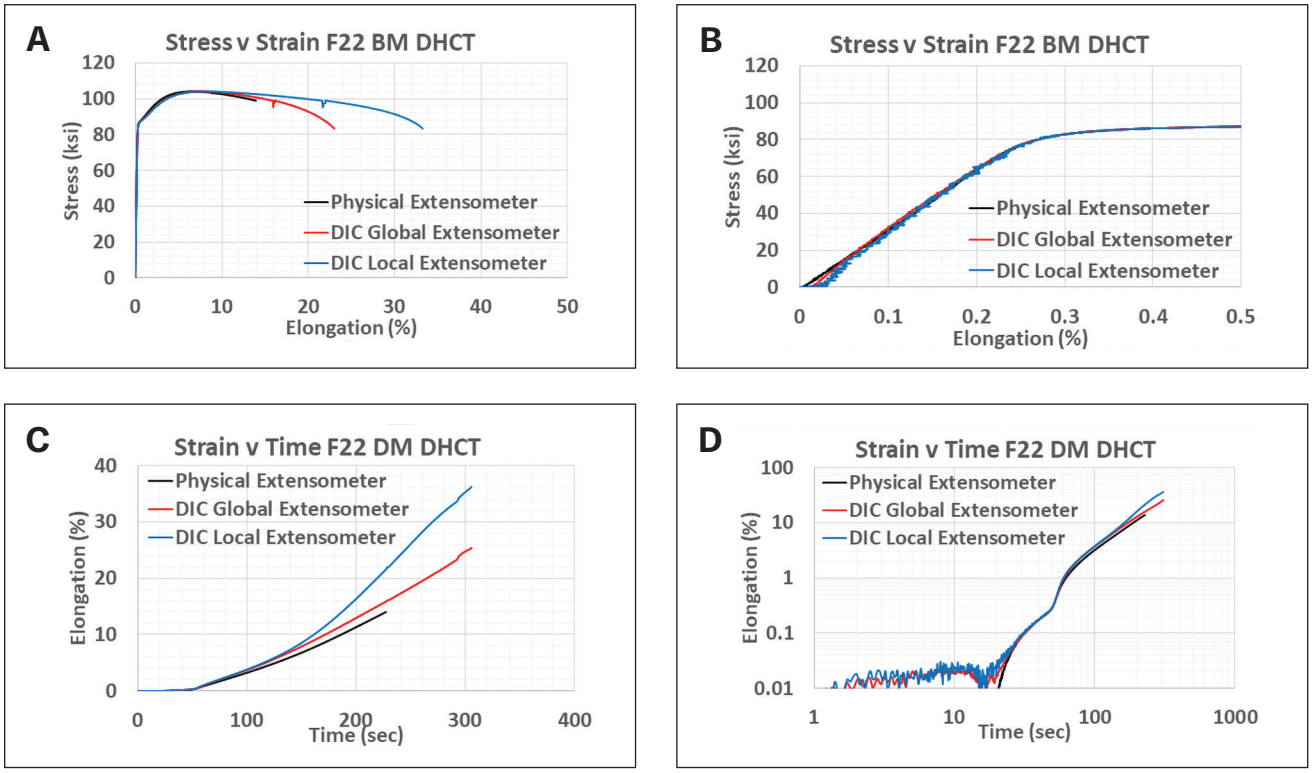

Fig. 5 — Comparison of DIC and physical extensometers in tensile testing F22 BM DHCT sample. A and B — Stress-strain curves; C and D — strain-time curves.

Table 3 — Test Samples and Extensometers

Sample ID	Test	Sample Geometry	Extensometer Locations/Dimensions (in.)				
			Physical	DIC Global	DIC Local		
F22 BM	Base metal tension	ASTM E8	0.75 × 1	0.25 × 1	Necking area: 0.25 × 0.25		
		DHCT		0.375 × 1	Necking area: 0.375 × 0.25		
F65/625 CWTT	Cross weld tension	DHCT			WM and BM: 0.375 × 0.5	FB: 0.375 × 0.1	HAZ: 0.375 × 0.25

tensile properties that were determined using the physical and DIC global extensometers. Note that the F22 DHCT samples produced a higher YS than the F22 dog bone samples. This YS difference can be related to the different ASTM E8 dog bone and DHCT sample geometries. Previous research has demonstrated the effect of sample geometry on tensile test results (Refs. 21–23). Figure 7 shows that at reaching the dog bone sample's yielding point (around 0.2% strain), the DHCT sample was well below this value at strain around 0.02%. At the DHCT sample's yielding point, the dog bone sample's plasticly strained to around 1%. This result shows that ASTM E8–determined BM YS can be used for selecting DHCT loads and would not cause macro-scale yielding in the tested F65/625 DMW.

Figures 4 and 5 show full overlapping curves of the physical, DIC global, and DIC local extensometers up to reaching the UTS points in the F22 BM dog bone and DHCT samples. The physical and DIC global extensometers closely overlap up to the point of physical extensometer removal. After reaching the UTS points, the local DIC extensometers measured strain concentration in the local necking areas, showing accelerated local strain accumulation (Figs. 4C and 5C). The dog bone sample showed similar global and local strain at failure, respectively, at 31.5 and 28% (Fig. 4 and Table 4). The local strain at failure in the DHCT sample was significantly

Table 4 — F22 BM and F65/625 DMW Tensile Properties Determined Using Physical and DIC Global Extensometers

Material	Sample Geometry	Extensometer	0.2% YS (ksi)	UTS (ksi)	Calculated Elastic Modulus (ksi)	% Error Physical vs. DIC Elastic Modulus (ksi)	Strain at Failure (%)
F22 BM	Dog bone 1	Physical	80	97.7	30627	2.4%	32.0
		DIC	80		31382		
	Dog bone 2	Physical	81	97.6	31067	0.2%	31.5
		DIC	81		30999		
	Dog bone 3	Physical	Slip	95.6	Slip	NA	32.0
		DIC	80		30756		
	DHCT	Physical	86	104.3	30384	4.7%	25.3
		DIC	87		28964		
F65/625 CWTT	DHCT	Physical	81	99.1	33589	7.8%	54.6
		DIC	81		30985		
Notes	Slip = Physical extensometer slipped during testing						

higher than the global strain, 33 vs. 23%. In this study, the local strain accumulation in the necking areas of the dog bone and DHCT samples was quantified over 0.25 in. local gauge lengths. DIC-instrumented tensile testing allows for post-testing selection of local gauge lengths, which could be used for studying local strain hardening kinetics between the UTS and final failure points.

The results of F22 steel BM tensile testing with physical and global DIC extensometers validated the utilized DIC procedure for determining local mechanical behavior in CWTT.

DIC-Instrumented CWTT

The results in Fig. 6 and Table 5 clearly demonstrate the capacity of DIC-instrumented CWTT in determining local mechanical behavior, including YS, strain hardening kinetics, and elongation at failure in a weldment with steep compositional and microstructural gradients. The tested DMW is a typical example of an undermatching WM weldment. The tested heat of F65 steel had a materials testing report YS of 78 ksi. The CWTT on the DHCT sample geometry confirmed a lower WM YS compared to the BM, HAZ, and FB — Fig. 6B and Table 5.

The local DIC extensometers allowed determination of the kinetics of yielding and strain hardening in the tested DMW. The softer Alloy 625 WM was the first to reach yielding, followed by the dissimilar FB region, HAZ, and BM, as shown in Figs. 6B and D and Table 5. At BM yielding, the HAZ, FB region, and WM were already strained to 0.31, 0.34, and 0.46%, respectively. Between yielding and 1% elongation, the WM exhibited the fastest strain hardening, followed by the FB region, HAZ, and BM — Fig. 6C.

As the tensile loading progressed, the BMs and WMs strain hardened with alternating pace up to about 16% elongation, at which point the WM strengthened enough to force necking in the BM at 18.5% elongation — Figs. 6A, C, and D and Table 5. The HAZ and FB experienced less strain hardening, reaching 10.5 and 10.6% elongation at base metal necking. The lower response to strain hardening in these regions is related to the formation of hard microstructural constituents during welding (Refs. 24–28). After the onset of necking, the BM elongated 54.6% to fail at a load of 85 ksi. After BM necking, the WM, HAZ, and FB region experienced additional elongation — Figs. 6A, C. The WM elongated only 0.6% between the BM necking and failure. This is an indication that at reaching the BM necking point, the WM strain hardened close to its UTS. The FB and HAZ experienced larger elongation, demon-

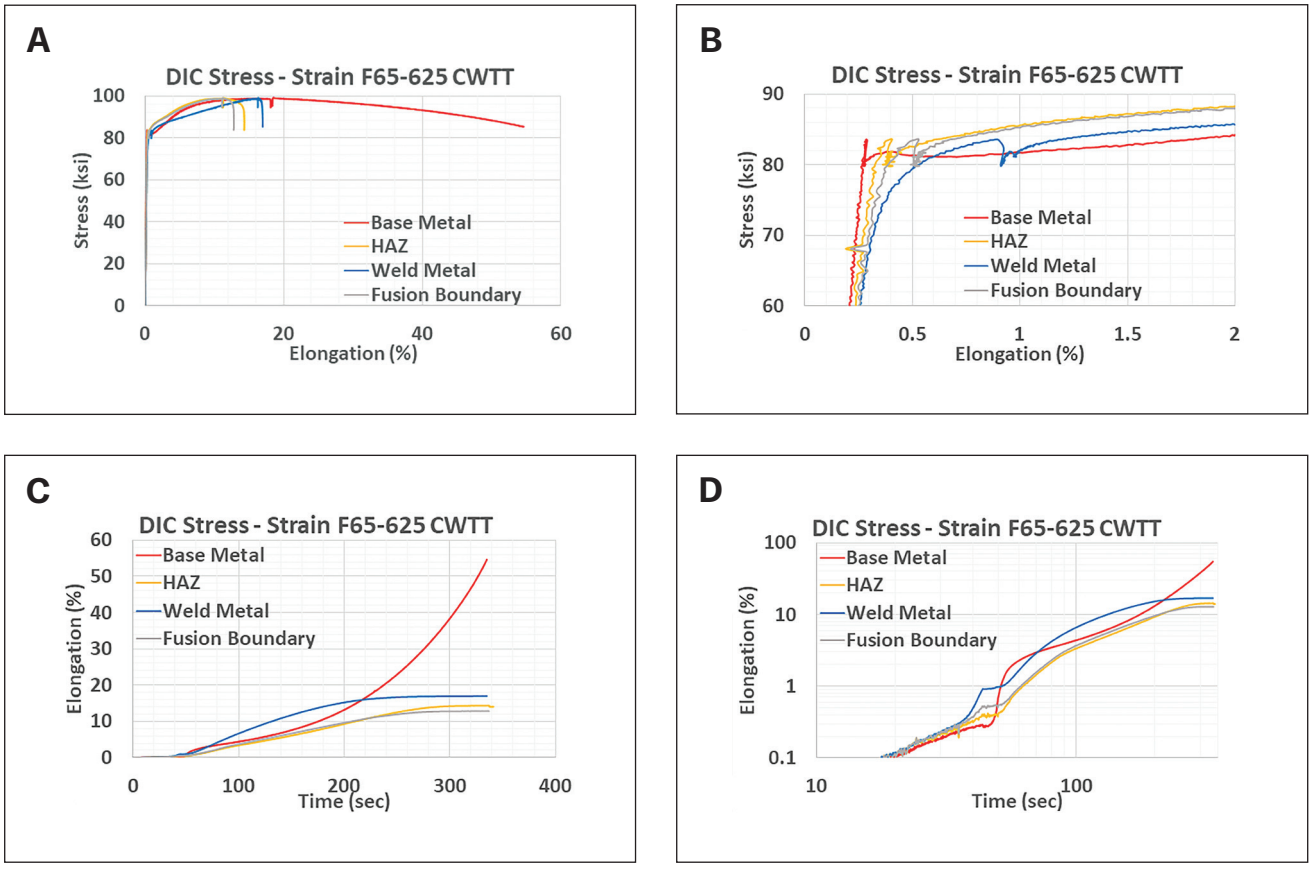

Fig. 6 — DIC quantification of the local mechanical behavior during CWTT of F65/625 dissimilar-metal weld. A and B — Stress-strain curves; C and D — strain-time curves.

Table 5 — DIC-Instrumented CWTT: Local Tensile Properties in F65/625 Dissimilar-Metal Weld

Welment Zone	Strain (%) at Testing Loads				YS, ksi	UTS, ksi
	BM YS	BM UTS	BM Failure	Absorbed Mech. Energy (J)		
BM	0.28	18.5	54.6	47.6	82	99.1
HAZ	0.31	10.5	13.5	11.6	81	
FB	0.34	10.6	12.8	11.5	80	N/A
WM	0.46	16.3	16.9	13.5	78	

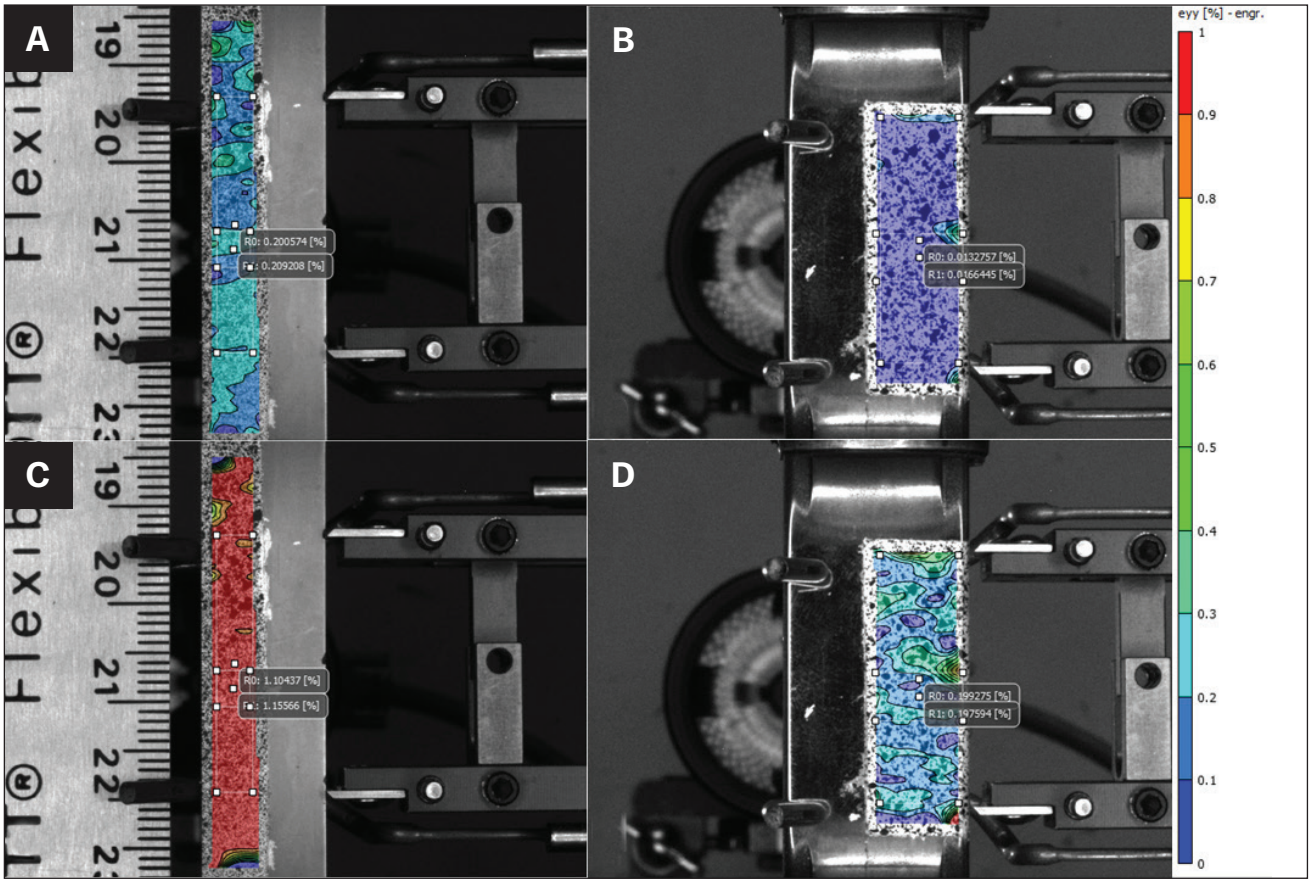

Fig. 7 — DIC strain maps and global and local extensometer strain values in the ASTM dog bone sample (A, C) and DHCT sample (B, D). A and B — At dog bone sample 0.2% strain; C and D — at DHCT 0.2% strain.

strating higher strain hardening capacity and potentially higher UTS values (Table 5). By recording the local stress-strain curves, the application of DIC in CWTT allowed for quantification of the absorbed mechanical energy in the BM, WM, HAZ, and FB regions (Table 5). The energy absorbed by the BM represents its fracture toughness.

The performed DIC-instrumented CWTT revealed the strain hardening mechanism behind BM failure in a DMW with undermatching WMs. Based on current code requirements, WM undermatching or overmatching conditions are defined by the BM and all WM tensile testing, while CWTT only determines the UTS of a weldment and verifies weld quality by BM failure.

The results of this study indicate that DIC-instrumented CWTT can be successfully utilized in determining the local mechanical behavior in both dissimilar– and matching–filler metal welds. This testing approach could provide valuable insight in the service performance of weldments with varying cross-weld microstructures and mechanical properties related to BM and WM chemical composition, welding, and postweld heat treatment procedures. Applications of interest could be related to strain-based design and HAZ softening in welds of thermomechanically controlled processed steels. In terms of evaluating hydrogen cracking susceptibility in DMWs, DIC-instrumented CWTT can be used to select DHCT loads that avoid local yielding in the tested DMW and quantify local elastic strain distribution at the applied DHCT load. Ongoing research has indicated elastic strain concentration in the FB region of DMWs is susceptible to HAC.

Summary and Conclusions

The applied DIC testing procedure provided equal results with a conventional physical extensometer in terms of YS, elastic modulus, and straining kinetics over the same gauge length in ASTM dog bone samples and in NACE DHCT samples.

DIC-instrumented tensile testing of homogeneous materials allows post-testing establishment of multiple virtual extensometers that can be used to quantify local mechanical behavior as strain-hardening kinetics and strain at failure in the necking area.

DIC-instrumented CWTT allows for quantification of the local YS, kinetics of strain hardening, and strain at failure in the BM, HAZ, FB region, and WM in matching- and dissimilar-metal welds.

DIC-instrumented CWTT can be utilized for determining the WM undermatching/overmatching condition and for evaluation of service performance in undermatching WM weldments.

The F65 steel BM failure in CWTT of the tested F65/Alloy 625 undermatching DMW was due to the rapid strain hardening response in the Alloy 625 WM.

DIC-instrumented CWTT can be used in quantifying the local elastic strain distribution in DMWs during testing HAC susceptibility with the DHCT, thus providing a new capability for studying the HAC phenomenon.

Acknowledgments

This research was performed within the National Science Foundation Manufacturing and Materials Innovation Joining Center (Ma2JIC) and supported by TechnipFMC. This research was also supported by Thomas Riss and Hongye Chen through sample preparation and testing setup assistance.

References

1. AWS B4.0:2016-AMD1, *Standard Methods for Mechanical Testing of Welds*. 8th edition. Miami, Fla.: American Welding Society.

2. E28 Committee. *Standard Test Methods for Tension Testing of Metallic Materials*. ASTM International. Accessed July 18, 2022. DOI: 10.1520/E0008_E0008M-16A

3. E28 Committee. *Test Methods for Young's Modulus, Tangent Modulus, and Chord Modulus*. ASTM International. Accessed November 28, 2022. DOI: 10.1520/E0111-17

4. A01 Committee. *Standard Test Methods and Definitions for Mechanical Testing of Steel Products*. ASTM International. Accessed July 18, 2022. DOI: 10.1520/A0370-6621

5. API. *Welding of Pipelines and Related Facilities*. Washington, DC: American Petroleum Institute (API).

6. AWS D1.1/D1.1M: 2015, *Structural Welding Code — Steel*. Miami, Fla.: American Welding Society.

7. Siefert, W., Rule, J., Alexandrov, B., Buehner, M., and Penso, J. A. 2020. Cross weld tensile testing with digital image correlation to determine local strain response. *PVP2020* Vol. 6: Materials and Fabrication. DOI: 10.1115/PVP2020-21580

8. Kulkarni, A., Dwivedi, D. K., and Vasudevan, M. 2020. Microstructure and mechanical properties of A-TIG welded AISI 316L SS-Alloy 800 dissimilar metal joint. *Materials Science & Engineering A* 790: 139685. DOI: 10.1016/j.msea.2020-139685

9. Tao, H., Tong, W., Hector, L. G., and Zavattieri, P. D. 2008. Uniaxial tensile and simple shear behavior of resistance spot-welded dual-phase steel joints. *Journal of Materials Engineering and Performance* 17(4): 517–534. British Library Document Supply Centre Inside Serials & Conference Proceedings. DOI: 10.1007/s11665-007-9170-8

10. Ghadbeigi, H., Pinna, C., Celotto, S., and Yates, J. R. 2010. Local plastic strain evolution in a high strength dual-phase steel. *Materials Science & Engineering A* 527(18–19): 5026–5032. DOI: 10.1016/j.msea.2010.04.052

11. Kang, J., Ososkov, Y., Embury, J. D., and Wilkinson, D. S. 2007. Digital image correlation studies for microscopic strain distribution and damage in dual phase steels. *Scripta Materialia* 56(11): 999–1002. DOI: 10.1016/j.scriptamat.2007.01.031

12. Wang, D.-Q., Zhu, M.-L., and Xuan, F.-Z. 2017. Correlation of local strain with microstructures around fusion zone of a Cr-Ni-Mo-V steel welded joint. *Materials Science & Engineering A* 685: 205–212. DOI: 10.1016/j.msea.2017.01.015

13. Paul, S. K., Roy, S., Sivaprasad, S., Bar, H. N., and Tarafder, S. 2017. Local ratcheting response in dissimilar metal weld joint: Characterization through digital image correlation technique. *Journal of Materials Engineering and Performance* 26(10): 4953–4963. DOI: 10.1007/s11665-017-2919-9

14. Sutton, M. A., et al. 1983. Determination of displacements using an improved digital correlation method. *Image and Vision Computing* 1(3): 133–139. DOI: 10.1016/0262-8856(83)90064-1

15. Sutton, M. A., et al. 1986. Application of an optimized digital correlation method to planar deformation analysis. *Image and Vision Computing* 4(3): 143–150. DOI: 10.1016/0262-8856(86)90057-0

16. Bruck, H. A., et al. 1989. Digital image correlation using Newton-Raphson method of partial differential correction. *Experimental Mechanics* 29(3): 261–267. DOI: 10.1007/BF02321405

17. Schreier, H., Orteu, J. J., and Schreier, H. W. 2009. *Image Correlation for Shape, Motion and Deformation Measurements: Basic Concepts, Theory and Applications*, 1–321. New York, N.Y.: Springer. DOI: 10.1007/978-0-387-78747-3

18. Chu, T. C., et al. 1985. Applications of digital-image-correlation techniques to experimental mechanics. *Experimental Mechanics* 25(3): 232–244. DOI: 10.1007/BF02325092

19. McNeill, S. R., Peters, W. H., and Sutton, M. A. 1987. Estimation of stress intensity factor by digital image correlation. *Engineering Fracture Mechanics* 28(1): 101–112. DOI: 10.1016/0013-7944(87)90124-X

20. Lippold, J. 2015. *Welding Metallurgy and Weldability*. Hoboken, N.J.: John Wiley & Sons Inc.

21. Mota-Solis, N., et al. 2013. Assessment of specimen geometry for all-weld metal tensile test in narrow groove welding. *Materials Technology; Ocean Space Utilization* Vol. 3. DOI: 10.1115/OMAE2013-10929

22. Savic, V., et al. 2012. Effects of gage section geometry on tensile material properties by digital image correlation. *SAE Technical Paper Series*. DOI: 10.4271/2012-01-0184

23. Wattrisse, B., Chrysochoos, A., Muracciole, J. M., and Nemoz-Gaillard, M. 2001. Analysis of strain localization during tensile tests by digital image correlation. *Experimental Mechanics* 41(1): 29–39. DOI: 10.1007/BF02323101

24. Alexandrov, B. 2012. A new test for evaluation of susceptibility to hydrogen assisted cracking in dissimilar metal welds. *NACE - International Corrosion Conference Series* 6: 4748–4758.

25. Bourgeois, D., and Alexandrov, B. 2022. Ranking the susceptibility to hydrogen-assisted cracking in dissimilar metal welds. *Welding in the World* 66(8): 1535–1550. DOI: 10.1007/s40194-022-01308-2

26. Alexandrov, B. T., Lippold, J. C., Sowards, J. W., Hope, A. T., and Saltzmann, D. R. 2013. Fusion boundary microstructure evolution associated with embrittlement of Ni–base alloy overlays applied to carbon steel. *Welding in the World* 57(1): 39–53. DOI: 10.1007/s40194-012-0007-1

27. Dai, T., and Lippold, J. C. 2018. The effect of postweld heat treatment on hydrogen-assisted cracking of 8630/Alloy 625 overlay. *Welding in the World* 62(3): 581–99. DOI: 10.1007/s40194-018-0578-6

28. Buntain, R., Alexandrov, B., and Viswanathan, G. 2020. Characterization of the interpass microstructure in low alloy steel/alloy 625 HW-GTAW narrow groove welds. *Materials Characterization* 170. DOI: 10.1016/j.matchar.2020.110638

WILLIAM SIEFERT (*siefert.24@buckeyemail.osu.edu*) and **DR. BOIAN ALEXANDROV** are with The Ohio State University, welding engineering, Columbus, Ohio. **MIKE BUEHNER** is with TechnipFMC, core technologies, Houston, Tex.